Timing analysis of the relationship between solar wind parameters and geosynchronous Pc5 amplitude

Kazue Takahashi[1] and Aleksandr Y. Ukhorskiy[1]

Received 15 April 2008; revised 23 July 2008; accepted 25 September 2008; published 5 December 2008.

[1] Solar wind-driven magnetospheric ULF waves in the Pc5 band (1.7–6.7 mHz) have been suggested to mediate the radial transport of electrons in the outer radiation belt. To identify the wave generation mechanism and the impact of the waves on the electrons, we performed correlation and superposed epoch analyses of the solar wind control parameters measured by the ACE spacecraft and the amplitude of Pc5 waves and the flux of radiation belt electrons measured at the GOES 12 geosynchronous satellite. The analyses were carried out for solar minimum year 2006, when the solar wind exhibited recurrent co-rotating interaction regions. We used hourly averages of solar wind velocity V_{sw}, the root-mean-square amplitudes of the solar wind dynamic pressure variations in the Pc5 band σP_{sw}, the azimuthal (σB_y) and compressional (σB_z) magnetic field components of geosynchronous Pc5 waves, as well as relativistic (>2 MeV) electron flux J_e at geosynchronous orbit. We found that σP_{sw} has a higher correlation with σB_y and σB_z than V_{sw} and that the correlation between σP_{sw} and the wave amplitudes peaks at or very near zero time shift. We conclude that the major driver of geosynchronous Pc5 waves is solar wind pressure variations rather than the Kelvin–Helmholtz instability on the magnetopause. Solar wind pressure pulses propagate into the inner magnetosphere at the MHD wave speed and it takes less than 1 hour for the signal to reach GEOS 12 from the bow shock nose. The pressure pulses also excite standing Alfvén waves that contribute to the σP_{sw}–σB_y correlation. There is a positive correlation between V_{sw} and Pc5 amplitude, but the correlation peaks at a time shift of about −1 day (the Pc5 peak occurs earlier than the V_{sw} peak). We attribute this shift to an intrinsic time shift between σP_{sw} and V_{sw}. J_e exhibits a minimum at the *Dst* minimum, coincident with the maximum of σP_{sw}, σB_y, and σB_z, and increases by 2 to 3 orders of magnitude over a period of about one day during which σB_y and σB_z decrease by one order of magnitude and V_{sw} reaches a peak value. However there are storms that do not exhibit electron flux enhancement despite the presence of strong Pc5 activity. Therefore the correlation between Pc5 amplitude and electron flux at geosynchronous orbit is not unique. The difference in electron response implies either the existence of other competing acceleration/loss mechanisms or that electron response to the Pc5 driver is nonlinear: similar driving conditions produce different response.

Citation: Takahashi, K., and A. Y. Ukhorskiy (2008), Timing analysis of the relationship between solar wind parameters and geosynchronous Pc5 amplitude, *J. Geophys. Res.*, *113*, A12204, doi:10.1029/2008JA013327.

1. Introduction

[2] The variation of the fluxes of energetic (energy > 1 MeV) electrons in the outer radiation belt (L range of approximately 3 to 7) has been a subject of intense research in recent years. One of the main drivers of the research is the recognition that the electron flux variations are not related to the global geomagnetic field variations that occur during geomagnetic storms (represented by the *Dst* index) in a simple manner. For example, a survey of radiation belt electron fluxes over a complete solar cycle [*Reeves et al.*, 2003] reported that geomagnetic storms can either increase or decrease the fluxes: only about half of all storms increased the fluxes, one quarter decreased the fluxes, and one quarter produced little or no change in the fluxes. Reeves et al. conclude that there is delicate balance between the amount of acceleration and the amount of loss for the electrons. To understand the behavior of the electrons, we need to quantitatively understand electron transport processes that result from both the immediate (time sales of minutes) and delayed (hours and days) magnetospheric responses to solar wind input.

[3] While our understanding of storm time magnetospheric processes remains far from complete, one can gain significant insight into the processes by examining the correla-

[1]Applied Physics Laboratory, Johns Hopkins University, Laurel, Maryland, USA.

0148-0227/08/2008JA013327

tions between various solar wind and magnetospheric parameters. It has been well known that the flux of energetic (~MeV) electrons measured at geosynchronous orbit (part of the outer radiation belt) is highly correlated with the velocity of the solar wind [*Paulikas and Blake*, 1979]. *Rostoker et al.* [1998] suggested that ultra-low-frequency (ULF) waves driven by the Kelvin–Helmholtz instability (KHI) on the magnetopause are responsible for the variation of the electron flux, based on a strong similarity in the time series of the intensity of Pc5 waves (1.7–6.7 mHz) observed on the ground and the flux of energetic electrons measured at a geostationary satellite. Theory indicates [e.g., *Fälthammar*, 1968] that magnetic and/or electric field oscillations in the Pc5 frequency range can violate the third adiabatic invariant of geomagnetically trapped electrons and may strongly contribute to the radial transport of the electrons if the waves have proper spatial and spectral properties. Many studies followed up the solar–wind–Pc5–electron relationship using both observational [*Mathie and Mann*, 2000a; *Green and Kivelson*, 2001; *O'Brien et al.*, 2001, 2003; *Posch et al.*, 2003] and theoretical [*Elkington et al.*, 1999; *Perry et al.*, 2005; *Fei et al.*, 2006; *Ukhorskiy et al.*, 2005, 2006a] approaches. Although these studies generally indicated that Pc5 wave-mediated electron transport is a viable process in the outer radiation belt, it is still not clear what the dominant generation mechanisms of the Pc5 waves is and how efficient they are in scattering radiation belt electrons. In this paper we compare the efficiency of various generation mechanisms of the Pc5 waves at geosynchronous orbit.

[4] Pc5 waves can be generated by both external and internal source mechanisms. The external mechanisms include buffeting of the magnetosphere by the solar wind dynamic pressure variations [*Kepko et al.*, 2002; *Mathie and Mann*, 2000b] and the KHI. The KHI excites both surface waves [*Southwood*, 1968; *Pu and Kivelson*, 1983] and body waves termed waveguide modes [*Samson et al.*, 1992; *Mann et al.*, 1999; *Mills et al.*, 1999] that propagate between the magnetopause and a turning point located in the magnetosphere. All of these external source waves couple to standing Alfvén waves in the magnetosphere [*Chen and Hasegawa*, 1974; *Southwood*, 1974; *Southwood and Kivelson*, 1990; *Mills and Wright*, 1999]. The internal mechanisms include drift mirror instability [*Hasegawa*, 1969] and drift–bounce resonances of ring current ions with standing Alfvén waves [*Southwood*, 1976].

[5] We investigate the relative efficiency of external source mechanism that are believed to be responsible for Pc5 waves with low (<10) azimuthal wavenumbers [*Ogilvie and Fitzenreiter*, 1989; *Matsuoka et al.*, 1995], which can exhibit drift resonance with radiation belt electrons [e.g., *Elkington et al.*, 1999] and therefore violate their third adiabatic invariant [e.g., *Ukhorskiy et al.*, 2005].

[6] While a positive correlation is generally found between solar wind speed (V_{sw}) and Pc5 amplitude in favor of the KHI, some studies noted a puzzling time delay between the arrival of fast solar wind speed streams and the onset of the Pc5 power enhancement. For example, *Engebretson et al.* [1998] reported that the peak wave power on the ground often occurred 1 day before the V_{sw} peaks. *Mann et al.* [2004] noted significant ULF wave power on the ground during the rising phase of solar wind velocity. *Vassiliadis et al.* [2007] found a time shift between the ULF wave power and V_{sw}.

[7] In a recent study [*Takahashi and Ukhorskiy*, 2007, hereinafter referred to as TU2007] we identified the solar wind dynamic pressure variations as a major driver of Pc5 waves observed at geosynchronous orbit. Using hourly parameters for both the solar wind bulk plasma parameters (propagated to the bow shock nose) and Pc5 power at geosynchronous orbit, we found that the power of dynamic pressure variations integrated over the Pc5 band had higher correlation with geosynchronous Pc5 power than V_{sw}. We compared the temporal profiles of solar wind and Pc5 parameters across a solar wind stream structure and noted that the peak of the Pc5 power occurred simultaneously with the peak of the power of the solar wind pressure variation but earlier than the peak of V_{sw}. We demonstrated that solar wind dynamic pressure variations excite toroidal standing Alfvén waves in addition to compressional oscillations that are a direct result of magnetosphere buffeting by dynamic pressure pulses. In a paper just published, *Kessel* [2008] reported a study that supports the result of TU2007.

[8] In this paper we conduct a statistical analysis of ACE and GOES data for 2006, a period around a solar minimum, and confirm the results of TU2007 obtained for 2001, a solar maximum year. The solar wind dynamics during 2006 were dominated by the recurrence of co-rotating interaction regions (CIRs) with solar wind velocity ranging from ~300 km/s to ~700 km/s. Since high-velocity (V_{sw} > 500 km/s) solar wind streams are identified as the main driver of the KHI [e.g., *Mann et al.*, 1999; *Claudepierre et al.*, 2008], these data are more suitable for addressing the possibility of the KHI than the time interval used in TU2007. An additional new aspect of the present study is the timing analysis of solar wind and Pc5 parameters. This analysis is motivated by the time shift between V_{sw} and Pc5 power noted above and provides further evidence that solar wind dynamic pressure variations are the dominant source mechanism of Pc5 waves at geosynchronous orbit and that the KHI play only a secondary role.

[9] The remainder of this paper is organized as follows. Section 2 describes the data. Discussion is presented in section 3, and the conclusions are presented in section 4.

2. Data

2.1. Data Set

[10] Data for this study come from the ACE spacecraft located at the Lagrangian point L1 and the GOES 12 spacecraft on a geostationary orbit. The ACE solar wind data used in this study were derived from the proton flux measured with the Solar Wind Electron Proton Alpha Monitor experiment [*McComas et al.*, 1998] and time shifted to the bow shock nose at the Space Physics Data Facility of NASA Goddard Space Flight Center. The data have been provided in 1-min time resolution. In 2006, GOES12 was located at ~75° West geographic longitude, which corresponded to a magnetic latitude of 10.5° and a local time (LT) and universal time (UT) relationship of LT = UT–5 h. The GOES 12 magnetic field data used in this study are also 1-min averages of vector samples acquired with a fluxgate magnetometer [*Singer et al.*, 1996] and provided by NOAA at http://www.swpc.noaa.gov/Data/

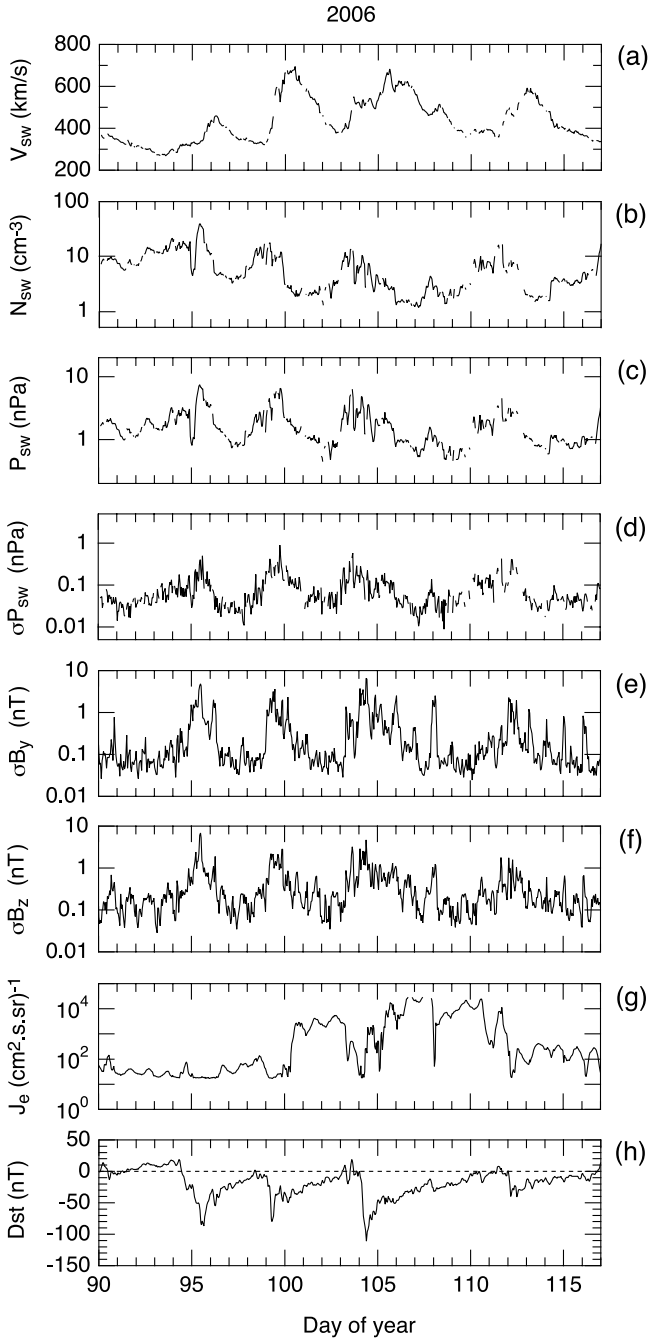

Figure 1. Twenty-seven-day plots of solar wind parameters from ACE (propagated to the bow shock nose), magnetic pulsation parameters, and electron flux at GOES 12, and the *Dst* index. See text for the definition of the parameters.

goes.html. We have rotated the magnetic field vector samples into a coordinate system referenced to the T89c model magnetic field [*Tsyganenko*, 1989]. In this system, B_x, B_y, and B_z represent the radial, azimuthal, and compressional components, respectively, where $\boldsymbol{e}_z$ is along the model magnetic field and $\boldsymbol{e}_x$ and $\boldsymbol{e}_y$ are perpendicular to it. As a result of a format problem in the original data file, the B_z component had a high digitization step equivalent to a root-mean-square amplitude of 0.2 nT when the field magnitude exceeded 100 nT, as described by TU2007. In addition we used the GOES 12 energetic (energy > 2 MeV) electron flux data that were included the magnetic field data files. GOES12 entered the magnetosheath once in 2006, and this interval was excluded from the analysis.

2.2. Solar Wind and Pc5 Parameters Over a Solar Rotation

[11] Figure 1 shows hourly solar wind and magnetospheric parameters for one solar rotation period (27 days) in 2006. Figures 1a–1d show the proton bulk velocity V_{sw}, proton number density N_{sw}, dynamic pressure P_{sw} ($= N_{sw}M_pV_{sw}^2$, where M_p is proton mass), and the root-mean-square amplitude of the oscillating component of P_{sw}, which is defined as the square root of the integral of the power spectral density (PSD) of P_{sw} over the Pc5 frequency band as

$$\sigma P_{sw} = \left(\int_{1.7\text{mHz}}^{6.7\text{mHz}} PSD\_P_{sw}(f)df \right)^{1/2} \quad (1)$$

[12] We subtracted the best-fit second-order polynomial from the original time series prior to computation of the PSD by Fourier transforming the input time series. It is likely that the P_{sw} variations are caused not by waves but by density and velocity fluctuations imbedded in the plasma. Even if they are waves, their propagation speed in the solar wind plasma rest frame is likely much slower than the solar wind speed seen from the Earth frame. This implies that the frequency of the observed P_{sw} oscillations is approximately given by λ/V_{sw}, where λ is the length scale of the P_{sw} structures. The solar wind data in Figure 1 are characterized by CIRs consisting of four high-speed streams. The peak V_{sw} values are 460, 680, 680, and 590 km/s. Each V_{sw} peak is preceded by ~1 day by a peak of N_{sw}, P_{sw}, and σP_{sw}.

[13] Figures 1e and 1f show Pc5 wave root-mean-square amplitudes σB_y and σB_z defined as

$$\sigma B_y = \left(\int_{1.7\text{mHz}}^{6.7\text{mHz}} PSD\_B_y(f)df \right)^{1/2} \quad (2)$$

$$\sigma B_z = \left(\int_{1.7\text{mHz}}^{6.7\text{mHz}} PSD\_B_z(f)df \right)^{1/2} \quad (3)$$

[14] The time series of σB_y and σB_z are nearly identical to each other and closely track σP_{sw} without any discernible time delay. The main difference between the time series of σP_{sw} and the pulsation amplitudes (σB_y and σB_z) is the existence of spikes separated by 24 hours in the latter. As described in TU2007, the spikes in σB_y occur when the spacecraft is on the nightside and are attributed to substorms. The spikes in σB_z occur at noon as a result of strong compression of the magnetic field in response, at this local time, to changes in the solar wind dynamic pressure. The large digitization noise, equivalent to a root-mean-square amplitude of ~0.2 nT, mentioned in section 2.1, also contributes to the σB_z enhancement on the dayside.

[15] Figure 1g shows the flux of energetic (energy > 2 MeV) electrons, J_e, at GOES 12. The electron flux was

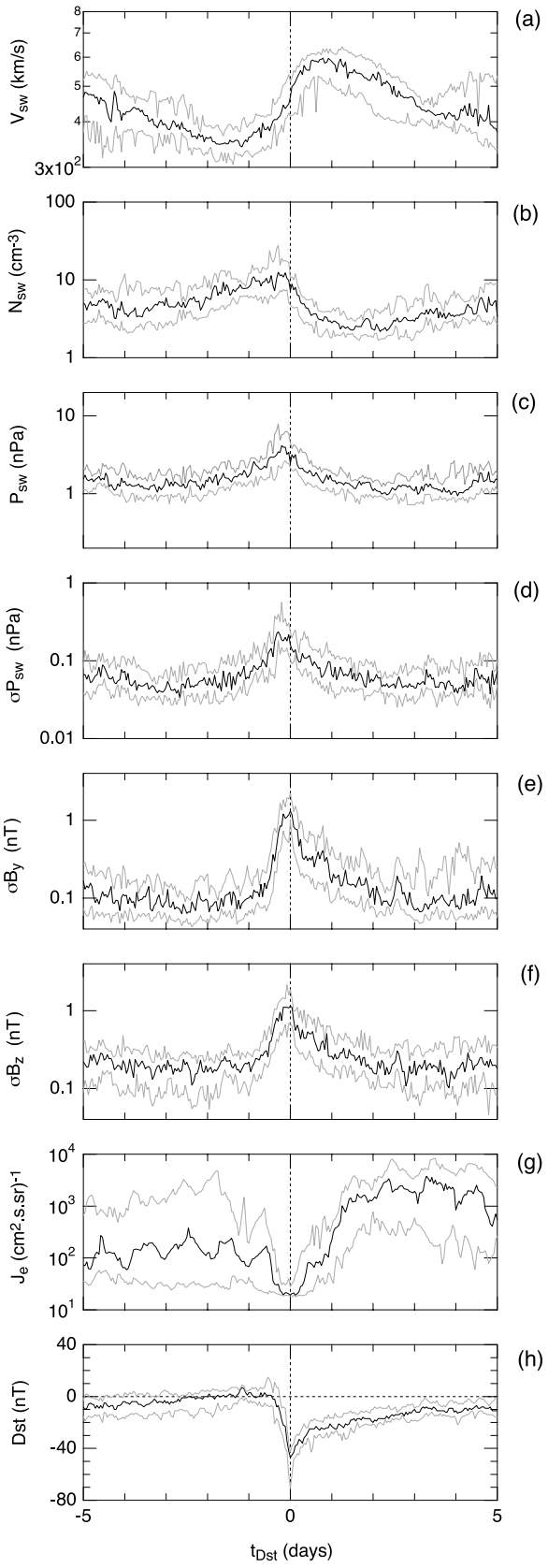

Figure 2. Superposed epoch analysis of hourly parameters from solar wind (ACE), magnetosphere (GOES 12), and *Dst* for 2006. Twenty-three storms entered the plot with zero epoch time given by the *Dst* minimum.

measured by a solid-state detector directed westward with a field of view of 2.0 radians. The flux varied by 3 orders of magnitude between $\sim$10 (cm^2·s·str)$^{-1}$ and $\sim 10^4$ (cm^2 · s · str)$^{-1}$ during the second and third geomagnetic storms (days 100–112) that are identified in the *Dst* plot (Figure 1h). These two storms were associated with peak V_{sw} values that exceeded 600 km/s. By contrast, there was only little change in the electron flux during the first storm (days 93–98) despite the fact that the *Dst* minimum (~ -85 nT) for this storm was comparable to those (-80 nT, -111 nT) of the second and third storms. During the fourth storm (days 112–117) the *Dst* minimum was only -40 nT, but there was a moderate enhancement of J_e to 10^2 (cm^2 · s · str)$^{-1}$. It is not clear why the first and fourth storms did not produce elevated J_e although we see lower V_{sw} peaks for these storms. The Pc5 amplitude at GEOS 12 was at a similar level among the four storms, so the Pc5 amplitude does not appear to be the major controlling factor of J_e. In confirmation of previous studies [e.g., *O'Brien et al.*, 2003], we also note anti-correlation between σB_y (and σB_z) and J_e. For example, the J_e minimum on day 104 is associated with a maximum of σB_y and σB_z, and the J_e maximum on day 103 is associated with a minimum of σB_y and σB_z.

[16] In the present study we do not make a distinction between broadband and narrowband Pc5 waves. Field variations arising from irregular oscillations driven by solar wind dynamic pressure pulses, toroidal standing Alfvén waves, and time-varying field aligned currents associated with substorms all contribute to the integrals given by expressions (2) and (3). TU2007 did separate out narrowband azimuthal field oscillations that most likely come from the fundamental toroidal standing Alfvén waves and showed that this narrowband component behaved quite similarly to the total band-integrated Pc5 intensity in terms of the dependence on the solar wind parameters. The reason for the similarity is that solar wind dynamic pressure pulses routinely excite toroidal waves. Therefore, in this study, we assume that the band-integrated σB_y exhibit similar dependence on the solar wind control parameters as toroidal waves.

2.3. Superposed Epoch Analysis

[17] To better characterize the relative timing of the variation of various parameters shown in Figure 1, we performed a superposed epoch analysis of the hourly parameters used in Figure 1 for the whole year 2006. The results are shown in Figure 2. In this analysis we identified 23 *Dst* minima in 2006 that were equal to or lower than -40 nT and following *O'Brien et al.* [2001, 2003] chose the time of the minima as the zero epoch time, $t_{Dst} = 0$. In each panel of Figure 2 the heavy trace indicates the median and the thin traces the upper and lower quartiles. The upper and lower quartile values of the solar wind parameters do not differ much, which indicates that the CIRs were a highly repetitive phenomenon. CIRs are the nearly exclusive driver of geomagnetic storms during the late declining phase of the 11-year solar activity cycle [*Denton et al.*, 2006]. Since data from all GOES 12 local times were used in Figure 2, some of the vertical spread of σB_z, σB_y, and J_e come from the local time dependence of these parameters. However the magnitude of the diurnal variations is smaller than the

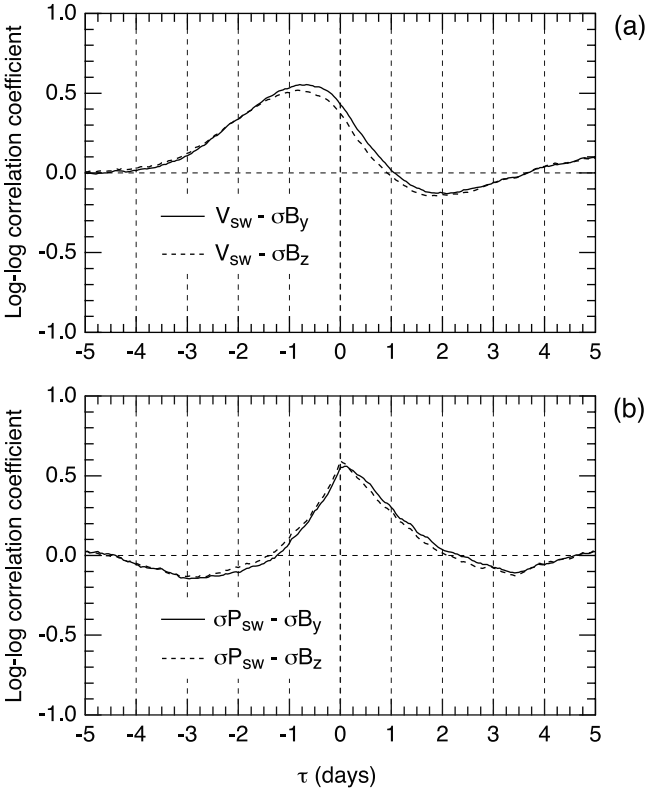

Figure 3. Cross correlation between solar wind parameters V_{sw} and σP_{sw} and GOES Pc5 amplitude σB_y and σB_z.

variations that are caused by the solar wind structure as seen in Figures 1e–1g.

[18] A few important observations can be made of Figure 2. First, a rapid rise of σB_y and σB_z occurs at $t_{Dst} \sim -0.5$ d, coincident with the sudden decrease of *Dst*. The peaks of σB_y and σB_z occur at $t_{Dst} \sim -0.1$ d, nearly coincident with the *Dst* minima ($t_{Dst} = 0$). Second, the peaks of N_{sw} and σP_{sw} occur simultaneously, and they coincide with the peaks of σB_y and σB_z. Third, the peak of V_{sw} occurs at $t_{Dst} \sim 1$ d and is broader than those of σP_{sw}, σB_y, and σB_z. Finally, the median electron flux has a minimum at $t_{Dst} = 0$, increases until $t_{Dst} = 1-2$ d, and stays at an elevated level for 3–4 d. The flux minimum has often been attributed to the adiabatic response (*Dst* effect) of the electrons to the magnetic field configuration changes associated with the development of storm time ring current [*Dessler and Karplus*, 1961; *Kim and Chan*, 1997]. However outside of $L = 5$ nonadiabatic loss mechanisms are considered to be more important [*Li et al.*, 1997]. For example, *Ukhorskiy et al.* [2006b] showed that deformation of electron drift orbits during storm main phase can lead to nearly complete loss of the electrons into the magnetopause outside $L \sim 5$. The electron flux exhibits a 24-hour variation, most evident in the median trace, which is attributed to local time sampling bias (J_e seen from a geostationary satellite has an intrinsic local time dependence since the geosynchronous orbit does not match the electron drift orbit). However the variation of J_e over the course of geomagnetic storms is much larger than the diurnal variation. Also, there are storms that are preceded by a high electron flux. This is seen in the traces of the upper quartile J_e and demonstrates the difficulty in relating the solar wind and magnetospheric ULF wave amplitude to the electron flux.

2.4. Cross Correlation Analysis

[19] The relative timing between geosynchronous Pc5 amplitude and solar wind parameters is further investigated using cross correlation analysis. Figure 3a shows the cross correlation of σB_y and σB_z versus V_{sw}, where the time shift (horizontal axis) is denoted τ. The two curves are nearly identical, which means that oscillations of both B_y and B_z respond quite similarly to the solar wind input. The correlation shows a peak value of 0.55 (for σB_y) or 0.52 (for σB_z) at $\tau \sim -0.8$ d, meaning that geosynchronous Pc5 amplitude on average leads V_{sw} by about 1 day. Figure 3b shows the cross correlation of σB_y and σB_z versus σP_{sw}. The σB_y and σB_z curves are once again nearly identical, but the peak correlation of 0.60 occurs at $\tau = 0$ for σB_z and the peak correlation of 0.56 occurs at $\tau = 0.1$ d for σB_y. This means that the response of Pc5 power to changes of σP_{sw} is essentially instantaneous.

[20] The result seen in Figure 3 can be easily explained by assuming that σP_{sw} is the main driver of geosynchronous Pc5 waves and that the time delay between the Pc5 amplitude and V_{sw} results from the intrinsic time delay between σP_{sw} and V_{sw}. Figure 4 shows the cross correlation of σP_{sw} versus V_{sw}. The peak correlation has a value of 0.52 and occurs at $\tau = -1.04$ d, which are nearly identical to the corresponding values seen in Figure 3a.

[21] The hourly solar wind and GOES Pc5 parameters are subjected to further statistical analyses to facilitate comparison with previous studies. Figure 5 shows scatter plots of all available samples of σP_{sw}, V_{sw}, σB_y and σB_z for 2006. Both σB_y and σB_z are positively correlated with σP_{sw} with log–log correlation coefficients of 0.56 and 0.60, respectively (Figure 5a). The V_{sw} dependence of σB_y and σB_z (Figure 5b) is weaker and results in moderate positive correlation coefficients of 0.43 and 0.47, respectively. Note that the local time variations of σB_y and σB_z seen in Figure 1 have amplitudes of less than 1 order of magnitude and thus make only a minor contribution to the variation shown here, which spans 2 orders of magnitude overall. Figure 5c demonstrates that σB_y are σB_z are highly correlated, an indication that they are controlled by a common source mechanism or mechanisms. The features seen Figures 5a–5c are consistent

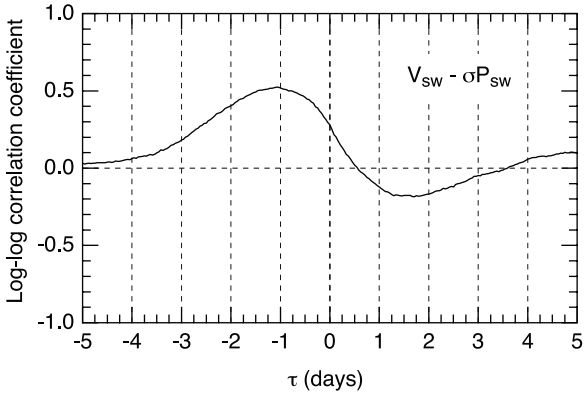

Figure 4. Cross correlation of σP_{sw} versus V_{sw}.

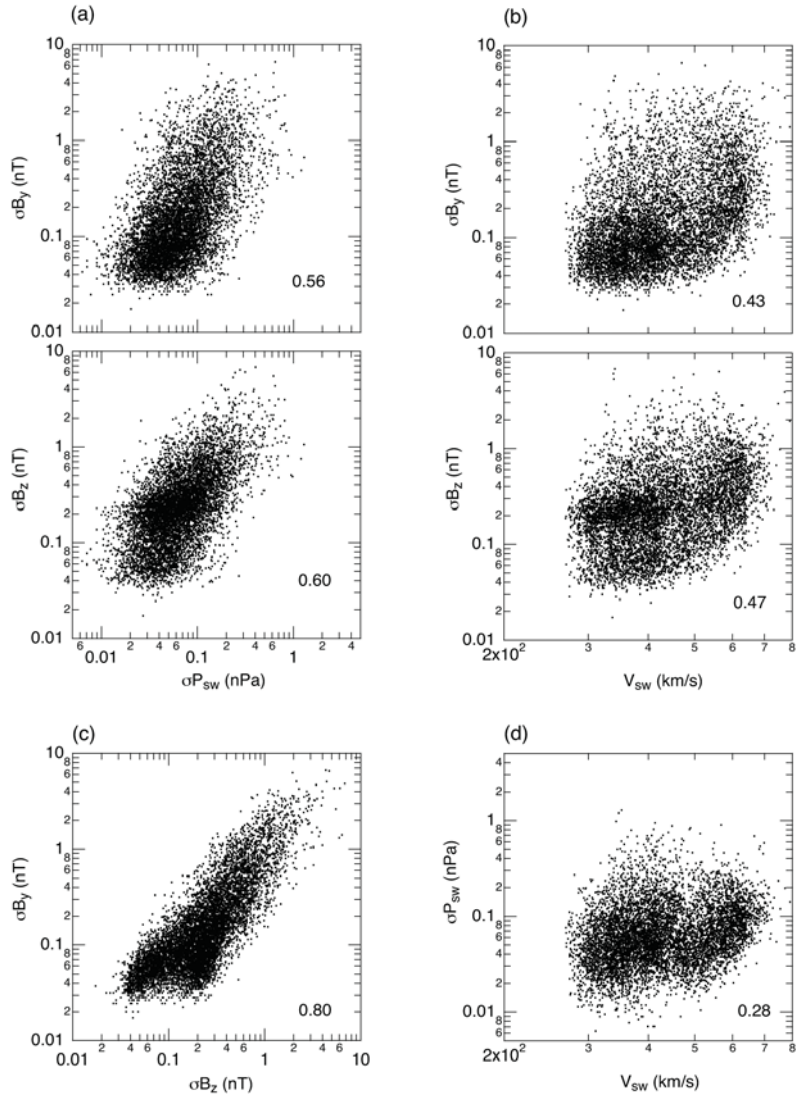

Figure 5. Scatter plots using all samples of hourly parameters σP_{sw} and V_{sw} from ACE and σB_y and σB_z from GOES 12 for 2006. The number in each panel indicates the log-log correlation coefficient between the parameters plotted. (a) Dependence of σB_y and σB_z on σP_{sw}. (b) Dependence σB_y and σB_z on V_{sw}. (c) Relationship between σB_y and σB_z. (d) Relationship between σP_{sw} and V_{sw}.

with the results obtained by TU2007 for the solar minimum year 2001. Finally, Figure 5d shows that the overall correlation between V_{sw} and σP_{sw} is low, with a correlation coefficient of 0.28. This may appear contradictory to what the time series plots in Figure 1 indicate: both V_{sw} and σP_{sw} exhibit quasiperiodic peaks associated with CIRs. However the apparent contradiction can be reconciled by noting that the peaks are time shifted and that slow variations (i.e., running averages over a few high speed streams) of σP_{sw} and V_{sw} are not correlated. The low correlation seen in Figure 5d between V_{sw} and σP_{sw} implies that we can take that these parameters (at zero time shift) are statistically nearly independent.

[22] We can extract additional information on the Pc5 waves by binning the hourly data. Figure 6a shows the result of correlation analysis after binning the data by the local time of GOES 12. This is a repeat of an analysis done in TU2007 for a solar maximum year 2001 using ACE and GOES 8 data and reproduced in Figure 6b. During the solar minimum year 2006 the σP_{sw} control is stronger than the V_{sw} control on both σB_y and σB_z. An exception occurs at 17–20 LT where the log–log correlation of $\sim$0.5 is found for both σP_{sw} and V_{sw}. During 2001 the σP_{sw} control was about the same but the V_{sw} control was lower at all local times, making σP_{sw} by far the dominant controlling parameter.

[23] We next binned the data by t_{Dst} as shown in Figure 7. This is motivated by previous studies that emphasized the role of Pc5 waves in electron transport during storm recovery [e.g., *O'Brien et al.*, 2001] and by studies that excluded storm onset from solar wind–pulsation correlation analysis [e.g., *Mathie and Mann*, 2000a]. Inspection of Figure 2 indeed suggests that t_{Dst} is useful for separating solar wind parameter regimes. For example, one regime is characterized by low V_{sw} and high N_{sw} and occurs prior to storm onset. Another regime is characterized by high V_{sw}

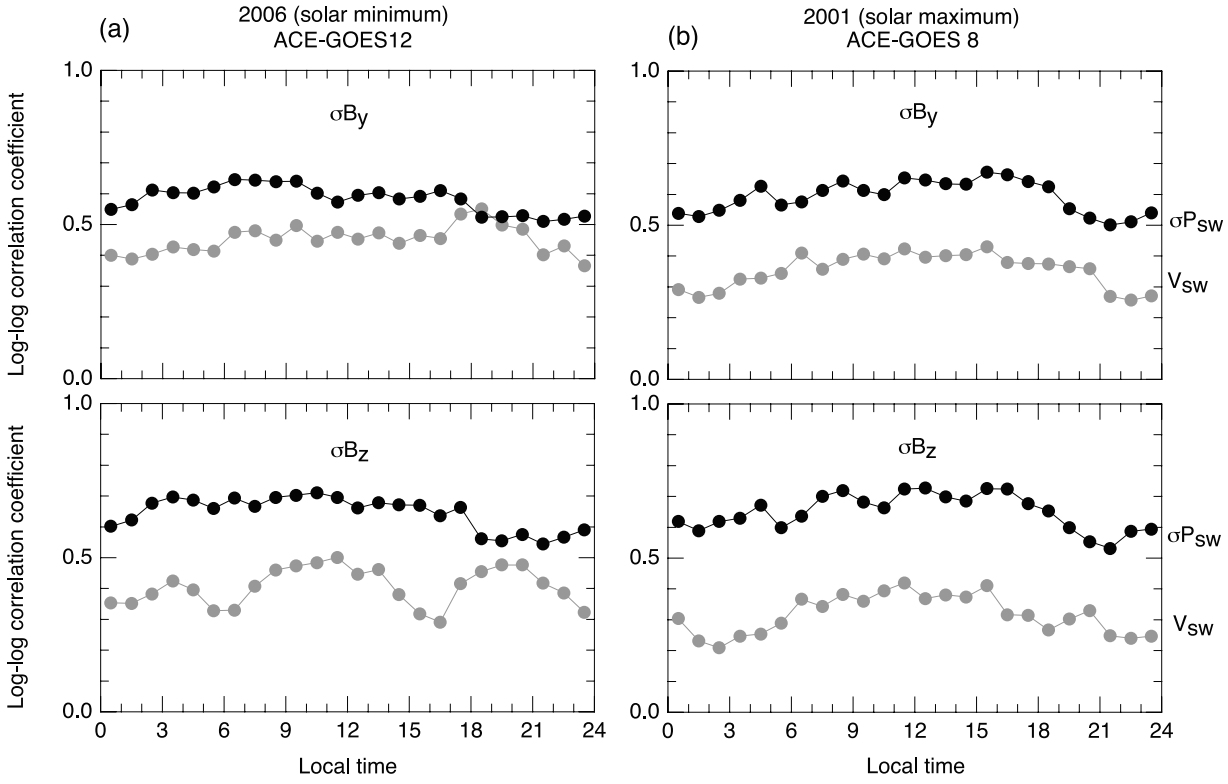

Figure 6. Local time dependence of the control of Pc5 pulsation amplitude in the B_y component (top) and B_z component (bottom) at geosynchronous orbit by solar wind parameters σP_{sw} and V_{sw}. (a) Result from the GOES 12 data for 2006 (solar minimum) used in the present study. (b) Result for the solar maximum year 2001 obtained using GOES 8 data, modified from Figure 9 of TU2007.

and low N_{sw} and occurs after storm onset. Considering the local time dependence of various possible source mechanisms we also separated GOES 12 location between dayside (0600–1800 LT, Figure 7a) and nightside (otherwise, Figure 7b). Furthermore, in each local time sector the azimuthal amplitude σB_y and compressional amplitude σB_z are examined separately.

[24] The four panels of Figure 7 show qualitatively the same t_{Dst} dependence of the correlation coefficients. Before the storm onset ($t_{Dst} < 0$) σP_{sw} exhibits much stronger control of both σB_y and σB_z than V_{sw}. At the storm maximum ($t_{Dst} = 0$), the V_{sw} control becomes very weak. However, during the recovery phase, from $t_{Dst} = 1$–2 d, the V_{sw} control becomes stronger and nearly equal to the σP_{sw} control. This coincides the time when V_{sw} reaches the peak value. Later in the storm recovery ($t_{Dst} > 2$ d) the V_{sw} control becomes low again, making σP_{sw} the stronger parameter.

3. Discussion

3.1. Driver of Pc5 Waves

[25] Cross correlation and superposed epoch analysis have been used in previous investigations of the causal relationship between solar wind condition, ULF waves, and the radiation belt electron fluxes. We took a similar approach but explicitly included σP_{sw} as a solar wind parameter in addition to the "dc" parameters V_{sw}, N_{sw}, and P_{sw}. Our analysis clearly demonstrates that σP_{sw} is strongly correlated with magnetospheric ULF wave amplitude and needs to be considered as a crucial solar wind parameter in studying excitation mechanisms of magnetospheric ULF waves.

[26] Regarding the σP_{sw} control of Pc5 amplitude, the first feature to note is that the Pc5 amplitude at geosynchronous orbit peaks simultaneously with σP_{sw}. This has been seen both in the superposed epoch analysis (Figure 2) and the cross correlation analysis (Figure 3). In the superposed epoch analysis the period of the most intense ULF waves occurs in the storm main phase when *D*st rapidly decreases. This relative timing can be most easily explained by assuming that magnetospheric Pc5 waves are directly driven by solar wind pressure variations.

[27] On average, the width of the σP_{sw} peak is about half a day, which corresponds to the time between the arrival of the leading edge of a high-V_{sw} stream (Figure 2a) and the start of the rapid decease of N_{sw} (Figure 2b). The peak value of the median σB_y is ~1.3 nT, which is greater than the pre-storm level ($t_{Dst} < 1$ d) of ~0.1 nT by a factor of ~13. The peak value of the median σB_z is ~1.1 nT, and the pre-storm value is ~0.2 nT, which is higher than for σB_y because of the digitization noise mentioned in section 2.1. At the peak of V_{sw}, which occurs at $t_{Dst} \sim 1$ d, we find $\sigma B_y \sim \sigma B_z \sim$ 0.3 nT, down from their peak values by a factor of ~3. This translates to approximately an order of magnitude power (= amplitude squared) reduction.

3.2. Time Shift Between V_{sw} and Pc5 Waves

[28] Previous statistical studies identified V_{sw} as the key solar wind control parameter of the ULF wave amplitude in

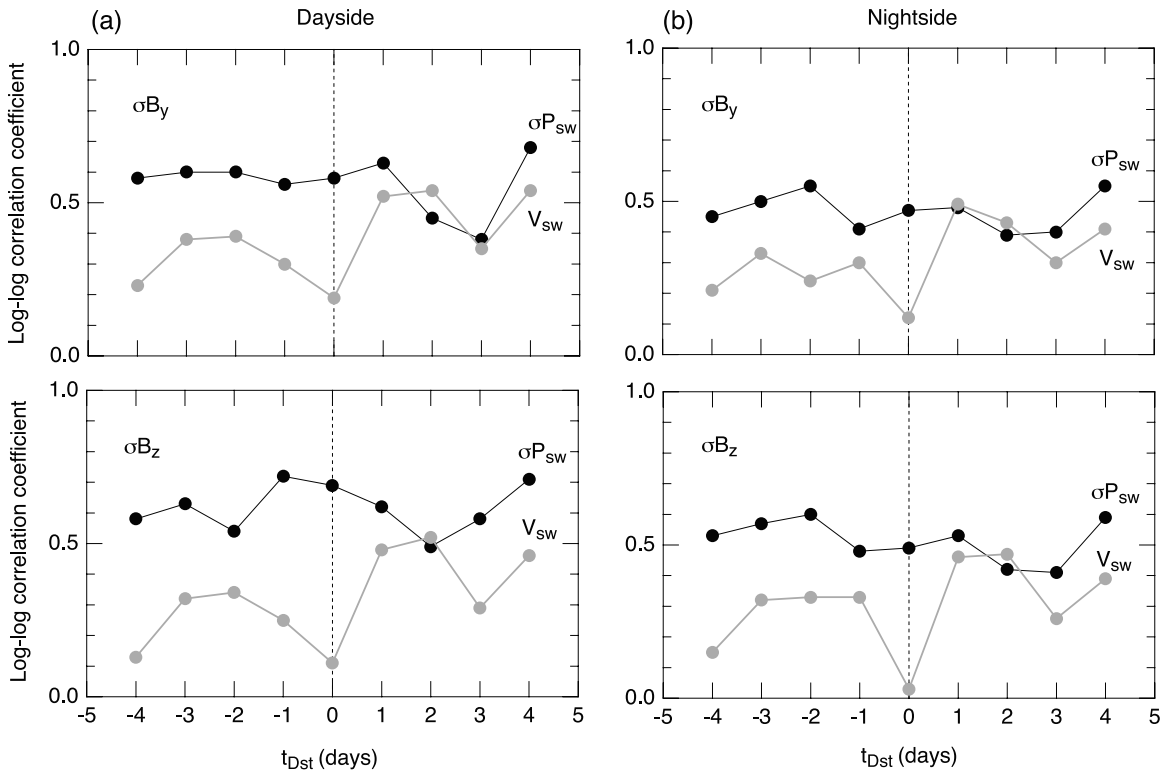

Figure 7. Log–log correlation coefficients between solar wind parameter (σP_{sw} or V_{sw}) and Pc5 amplitude at GOES 12 (σB_y or σB_z) as a function of t_{Dst}, the time from *Dst* minimum for 2006. The width of the t_{Dst} bins is 1 day. (a) Results for GOES 12 position on the dayside (0600–1800 LT, where LT = UT – 5 hours). (b) Results for GOES 12 position on the nightside (0000–0600 and 1800–2400 LT).

the magnetosphere [*Greenstadt et al.*, 1979; *Wolfe and Meloni*, 1981; *Junginger and Baumjohann*, 1988]. In these studies the KHI was usually suggested as the main mechanism for wave generation since the instability threshold at the magnetopause is more likely to be exceeded when the solar wind velocity is higher. Once the instability threshold is met, a wave can grow to substantial amplitude, controlled by the threshold value, in a few wave periods (tens of minutes). Thus a change in the instability threshold affects the distribution of the ULF wave amplitude in the inner magnetosphere almost immediately compared to the 1-hour time resolution used in this and other statistical studies.

[29] However some of previous studies reported a finite time shift (>1 h) between the peak ULF wave power and the peak V_{sw}, posing a potential problem in interpreting the observations with the KHI mechanism. For example, *Engebretson et al.* [1998] noted that wave power time series from the magnetometers at Cape Dorset (magnetic latitude 64.2°) and Kevo (69.8°) frequently led the V_{sw} time series by 1 day. *Engebretson et al.* [1998] provided an explanation for this time shift in terms of the dependence of the KHI threshold on the plasma mass density. For simplified magnetopause geometry, *Engebretson et al.* [1998]showed that the mass densities on both sides of the magnetopause have a non-negligible role in controlling the instability threshold. Thus the temporal profile of solar wind density shown in Figure 2 will correspond to the lowest V_{sw} threshold that occurs before the peak in V_{sw}. This timing difference was estimated to be about 0.5 day.

[30] More recently, *Vassiliadis et al.* [2007] reported in their Figure 4 a similar (15 h) timing difference between V_{sw} and Pc5 power on the ground and provided a different explanation. In this alternative scenario, the timing difference is attributed to strong absorption of wave power during the period of high V_{sw}. A possible mechanism of the absorption is wave–particle interaction, where the relevant particle population can be energetic electrons in the radiation belt, cold electrons in the plasmasphere, and ring current ions.

[31] In our view, the timing difference occurs simply because most of the time Pc5 waves are driven not by the KHI but by a sequence of P_{sw} pulses, which we envision to be distributed according the Kolmogorov spectrum [*Ukhorskiy and Sitnov*, 2008]. Buffeting of the magnetosphere by P_{sw} pulses has been documented by many authors [e.g., *Sarafopoulos*, 1995; *Matsuoka et al.*, 1995; *Kepko et al.*, 2002]. The pulses drive compressional magnetic field oscillations with waveforms identical to the applied pulses. These oscillations contribute to σB_z. In addition, damped standing Alfvén waves are excited with frequency locally determined by the plasma mass density and magnetic field. These waves contribute to σB_y as reported by TU2007.

[32] The magnetospheric consequence to P_{sw} pulses is well documented in theoretical studies. *Southwood and Kivelson* [1990] used an analytical approach to demonstrate that both forced compressional oscillations and standing Alfvén waves are excited in the magnetosphere in response to a finite-duration impulse applied on the outer boundary of

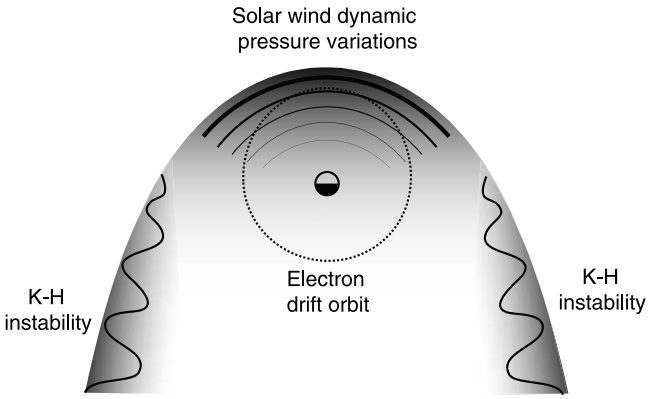

Figure 8. Schematic representing externally driven ULF waves in the magnetosphere. The dayside magnetosphere is filled with compressional magnetic pulsations driven by solar wind dynamic pressure variations. The amplitude of the pulsations is largest at the magnetopause nose but still is substantial at geostationary orbit. The Kelvin–Helmholtz instability generates surface waves on the magnetopause on the dawn and dusk flanks but their amplitude decays rapidly with distance from the generation region. The magnetopause is drawn in realistic shape and size based on *Shue et al.* [1998] magnetopause model with input parameters of $B_z = 0$ and $P_{sw} = 4.2$ nPa. A realistic drift orbit is shown for equatorial electrons.

the magnetosphere. A numerical simulation of the response of a dipole magnetosphere to a P_{sw} impulse [*Lee and Lysak*, 1989] demonstrated excitation of both global cavity waves and standing toroidal waves. Simulation studies of waveguide modes in simpler plasma geometry but with realistic random variations of the magnetopause position [*Wright and Rickard*, 1995a] or running pulses on the magnetopause [*Wright and Rickard*, 1995b] produced similar results. In the real magnetosphere the cavity/waveguide modes are hard to detect [e.g., *Waters et al.*, 2002], but there is abundant evidence in real data about the excitation forced compressional oscillations and the associated standing Alfvén waves.

[33] The dynamic pressure variations propagate from the bow-shock nose into the magnetosphere at approximately the Alfvén velocity, and the magnetospheric response time to the external disturbance will be of the order of 5 minutes, which explains the high correlation of σB_y and σB_z with σP_{sw} at or nearly at zero time shift. In addition, TU2007 have shown that the amplitude of dayside Pc5 waves has a local time dependence that matches field variations caused by the changes in the magnetopause Chapman–Ferraro current, in strong support of the direct solar wind source mechanism.

[34] There is no question that the KHI operates at the magnetopause or in the low-latitude boundary layer. Satellite observations have confirmed Pc5-band oscillations unique to the boundary region that are consistent with the KHI [*Takahashi et al.*, 1991; *Chen et al.*, 1993]. However how much energy this instability feeds to the geosynchronous region is unclear. The instability generates surface waves that decay with distance from the generation region. Unless the magnetosphere is highly compressed, the effect of the instability to Pc5 band waves at geosynchronous orbit may be quite limited. According to Figure 2c the peak median P_{sw} is 4.2 nPa ($t_{Dst} = -0.2$ d). At $t_{Dst} = 1.0$ d the median P_{sw} goes down to 1.8 nPa. This means that the magnetosphere expands from the storm main phase to the recovery phase, moving the KHI region away from the geosynchronous orbit. According to the model of *Shue et al.* [1998], the dawn and dusk magnetopause, the likely site of KHI, is located at 13.8 R_E for $P_{sw} = 4.2$ nPa and at 15.6 R_E for $P_{sw} = 1.8$ nPa, where we used $B_{zIMF} = 0$ as input to the magnetopause model. Correspondingly, a geosynchronous satellite located at 0600 LT sees the magnetopause about 7 R_E away at $t_{Dst} \sim 0$ and at about 9 R_E away at $t_{Dst} \sim 1$ d. This change in distance will tend to cancel out the effect of enhanced KHI waves at the time of peak V_{sw}. The limited influence of KHI surface waves on geosynchronous ULF power is also evident in a recent simulation study reported by *Claudepierre et al.* [2008]. We note that waveguide modes are body waves that propagate outside the turning point thus need not be localized to the close vicinity of the magnetopause. Interestingly, there is no clear indication of waveguide modes in the simulation of *Claudepierre et al.* [2008], at least in the Pc5 band. Perhaps the realistic geometry of the simulated magnetosphere makes it more difficult to excite waveguide modes than in the planer geometry employed in theoretical studies.

[35] Figure 8 schematically illustrates the spatial variation of ULF wave amplitude for the two source mechanisms discussed above. Solar wind pressure pulses produce compressional magnetic field oscillations that fill the dayside magnetosphere. The amplitude of these oscillations is strongest at the magnetopause nose and decreases toward the tail, but the amplitude is still substantial at geosynchronous orbit [*Matsuoka et al.*, 1995; *Ukhorskiy et al.*, 2006a; *Takahashi and Ukhorskiy*, 2007] (the closure current flowing in the magnetotail produces small perturbations that are in anti-phase with the dayside perturbations). Energetic electrons near geosynchronous orbit, whose drift orbit is illustrated in Figure 8 assuming mirroring at the magnetic equator, encounter the region of solar wind driven compressional pulsations over a wide range of local time. This interaction leads to changes of the energy and the drift shell of the electrons as demonstrated by a test particle simulation [*Ukhorskiy et al.*, 2006a].

[36] The KHI produces surface waves on the flanks of the magnetopause. The magnetopause is stable against this instability at the nose, where the solar wind speed is zero, and becomes unstable at the location where the velocity exceeds the threshold that is determined by the local plasma and magnetic field parameters on both sides of the magnetopause. Analytical studies as well as numerical simulations [*Wright and Mann*, 2006; *Claudepierre et al.*, 2008] indicate that the instability starts to grow at around dawn and dusk. However, as a result of the exponential decay of the surface waves excited by the KHI, the effect of the surface waves will be limited at geosynchronous orbit except when the magnetopause is highly compressed [*Takahashi et al.*, 1991] or when V_{sw} is very high so that KHI grows to substantial amplitude.

[37] We have shown in Figure 7 that around the time of V_{sw} peak (~1 day after the *Dst* minimum) the V_{sw} control of the geosynchronous Pc5 amplitude is elevated and becomes

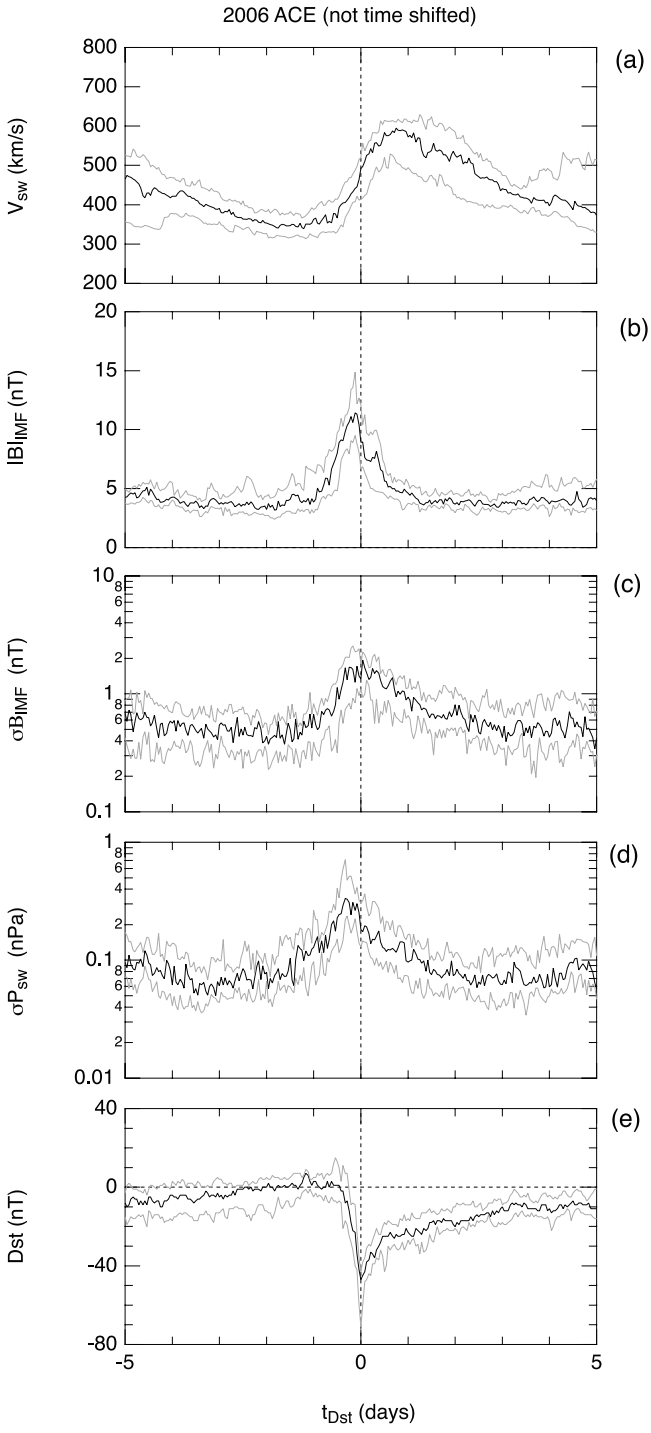

Figure 9. Superposed epoch analysis of solar wind plasma, solar wind magnetic field, and *Dst*. ACE data are not time shifted for this figure. The *Dst* plot is identical to that of Figure 2.

comparable to the σP_{sw} control. Therefore, at this particular phase of geomagnetic storms, V_{sw}-driven waves may play some role in radial transport/acceleration of energetic electrons in the outer radiation belt [*Rostoker et al.*, 1998; *O'Brien et al.*, 2001]. However it is not clear if the KHI is the cause of the elevated V_{sw} control. KHI-driven waves are considered dominant on the flanks and further tailward [*Wright et al.*, 2000; *Mills et al.*, 2000; *Wright et al.*, 2002] where the magnetosheath flow speed becomes close to the speed of the solar wind. Because the magnetosheath flow is stagnant at the magnetopause nose, the dayside magnetosphere is an unlikely region to be populated with waves generated by the KHI. Therefore it is difficult to explain the quite similar V_{sw} dependences seen on the dayside (Figure 7a) and on the nightside (Figure 7b) solely in terms of the KHI.

3.3. Correlation Between IMF Variations and Pc5 Waves

[38] *Kozyreva et al.* [2007] noted that the time series of ULF power of the interplanetary magnetic field (IMF) is quite similar to the time series of ground ULF power and that there is no time shift between the two. This finding motivated us to examine the relationship between σP_{sw} and IMF fluctuations. Figure 9 shows a superposed epoch analysis of the relevant parameters for 2006. For this figure we used non-time-shifted ACE data, but the average temporal profiles of V_{sw} and σP_{sw} are essentially identical to those shown in Figure 2 that used the time-shifted ACE data (the *Dst* plots are identical). In Figure 9 the amplitude of IMF oscillations, σB_{IMF}, is defined as

$$\sigma B_{IMF} = \left(\sigma B_{xGSM}^2 + \sigma B_{yGSM}^2 + \sigma B_{zGSM}^2\right)^{1/2} \quad (4)$$

where σB_{xGSM}, σB_{yGSM}, and σB_{zGSM} are Pc5-band amplitudes of the GSM components of the interplanetary magnetic field obtained using same integral as equations (2) and (3). Figures 7d and 7c indicate that the peaks of σP_{sw} and σB_{IMF} occur simultaneously, between $\tau = -0.5$ d and $\tau = 0$, although σB_{IMF} decays more slowly than σP_{sw}. This indicates that regions of intense variations in P_{sw} and IMF are collocated in the solar wind. Accordingly, σB_{IMF} can be used as a proxy of σP_{sw} in discussing Pc5 enhancement in the magnetosphere. However σB_{IMF} should be treated only as a marker of a disturbed region of the solar wind. The magnetic field variations do not produce strong pressure variations in the magnetosphere upon impact on the magnetopause. It is the dynamic pressure variations that exert the pressure variations that launch MHD waves into the magnetosphere.

3.4. Geosynchronous Electron Flux and Pc5 Waves

[39] Although both Pc5 wave amplitude and energetic electron fluxes are definitely related to the solar wind structure, it is not clear if there is a causal relationship between the waves and the electron fluxes. In the time series plots (Figure 1) we found that the electron flux may or may not increase during the storm recovery for similar types of Pc5 enhancement.

[40] The superposed epoch analysis (Figure 2) also indicated a wide range of electron flux variations both prior to and after the *Dst* minimum despite the fact that Pc5 amplitude exhibits a highly repetitive pattern with small variances about the median. As noted in Figure 2, the electron fluxes commonly show a minimum or dropout at the *Dst* minimum ($-0.5 < t_{Dst} < 0.5$ d), which coincides (within a timing error or less than 0.5 d) with the peak of Pc5 amplitude at GOES. Despite this timing agreement it is

not clear if Pc5 waves at *Dst* minimum play any significant role in the electron flux dropout. The dropout has been attributed to the adiabatic response of the electrons to rapidly reconfigured magnetic field in the ring current region [*Dessler and Karplus*, 1961; *Kim and Chan*, 1997] and to possible additional nonadiabatic losses [*Li et al.*, 1997] such as electron encounter with the magnetopause [*Ukhorskily et al.*, 2006a, 2006b]. In contrast, during the storm recovery ($t_{Dst} > 0.5$ days) the electron fluxes on average becomes higher than the prestorm level, which requires acceleration or radial transport of the electrons. During this period Pc5 waves are more likely to mediate the electron transport [e.g. *Rostoker et al.*, 1998].

[41] Two possible explanations can be suggested for the observed variability of the electron flux responses to the Pc5 wave activity during storm recovery. One commonly accepted theory suggests that the electron flux levels are determined by the superposition of multiple loss and acceleration mechanisms [e.g., *Friedel et al.*, 2002]. Relative contribution of various mechanisms may differ from storm to storm, producing a highly variable response in electron fluxes [*Reeves et al.*, 2003]. Recently however *Ukhorskiy et al.* [2006a] and *Ukhorskiy and Sitnov* [2008] showed that radial transport of radiation belt electrons because of Pc5 waves can exhibit large deviations from radial diffusion. Test particle simulations showed that electron motion becomes stochastic because of the overlap of electron populations trapped in the vicinities of drift resonances with adjacent harmonics of the field spectrum. However, in spite of the underlying stochasticity, the radial diffusion limit is not fully attainable in the outer radiation belt, because phase correlations in electron motion do not have time to decay because of the finite size of the system. As a result the electron flux varies nonlinearly: collective motion of the outer belt electrons can exhibit large deviations from radial diffusion.

[42] Finally, it is possible that the electron flux increase is caused by mechanisms not involving Pc5 waves. For example, *Nishimura et al.* [2007] showed that a time-dependent electric field in the inner magnetosphere derived from satellite observations can account for the recovery phase enhancement of relativistic electron fluxes observed at CRRES at $L = 5$. The electric field will depend on V_{sw}, which means we need to take such a mechanism into consideration in interpreting the V_{sw} dependence of electron fluxes in the outer radiation belt.

4. Conclusions

[43] We have studied the relationship among the solar wind parameters, magnetospheric Pc5 wave amplitudes, and flux of energetic electrons using data from the ACE and GOES 12 spacecraft for 2006, which was characterized by highly repetitive CIRs and the associated geomagnetic storms of moderate intensity. The results of data analysis can be summarized as follows.

[44] 1. Variations of the solar wind dynamic pressure, measured by the root-mean-square amplitude in the Pc5 frequency band (σP_{sw}), have higher correlation with magnetic wave amplitude in the Pc5 band (σB_y and σB_z) at geosynchronous orbit than the solar wind velocity V_{sw}.

[45] 2. The correlation between σP_{sw} and Pc5 amplitude (σB_y and σB_z) peaks at zero or near-zero time lag. This means that the pressure effect on the Pc5 waves is nearly instantaneous, which is explained by short propagation times ($\sim$5 min) of pressure pulses through the inner magnetosphere for fast magnetosonic waves.

[46] 3. The correlation between V_{sw} and Pc5 amplitude peaks with a time shift of about -1 day (the Pc5 peak occurs earlier than the V_{sw} peak). We explain this by taking σP_{sw} to be the true driver of the Pc5 waves and noting an intrinsic time delay between σP_{sw} and V_{sw}.

[47] 4. The geosynchronous electron flux exhibits a minimum at the storm maximum (= *Dst* minimum), which nearly coincides with the maximum of σP_{sw} and the associated maximum of the Pc5 wave amplitude. The flux minimum has been attributed to the adiabatic response of electrons to the global configuration change of the magnetic field (*Dst* effect) and also to loss mechanisms such as electron encounter with the magnetopause. Therefore the role of Pc5 waves in electron transport at this phase of storm is not clear. The electron flux increases by 2 to 3 orders of magnitude in a period of about one day, during which the wave amplitude decreases by one order of magnitude and solar wind velocity reaches a peak value. There are storm events that do not exhibit geosynchronous electron flux enhancement despite the presence of strong Pc5 activity. Therefore the correlation between Pc5 amplitude and electron flux at geosynchronous orbit is not unique, pointing to other mechanisms that contribute to the variations of the electron flux.

[48] **Acknowledgments.** This work was supported by NSF grant ATM-0540121. The authors are grateful to the referees for their constructive comments.

[49] Amitava Bhattacharjee thanks Andrew Wright and Patrizia Francia for their assistance in evaluating this paper.

References

Chen, L., and A. Hasegawa (1974), A theory of long-period magnetic pulsations: 1. Steady state excitation of field line resonance, *J. Geophys. Res.*, *79*(7), 1024–1032.

Chen, S. H., M. G. Kivelson, T. T. Gosling, R. J. Walker, and A. J. Lazarus (1993), Anomalous aspects of magnetosheath flow and the shape and oscillations of the magnetopause during an interval of strongly northward interplanetary magnetic field, *J. Geophys. Res.*, *98*(A4), 5727–5742.

Claudepierre, S. G., S. R. Elkington, and M. Wiltberger (2008), Solar wind driving of magnetospheric ULF waves: Pulsations driven by velocity shear at the magnetopause, *J. Geophys. Res.*, *113*, A05218, doi:10.1029/2007JA012890.

Denton, M. H., J. E. Borovsky, R. M. Skoug, M. F. Thomsen, B. Lavraud, M. G. Henderson, R. L. McPherron, J. C. Zhang, and M. W. Liemohn (2006), Geomagnetic storms driven by ICME- and CIR-dominated solar wind, *J. Geophys. Res.*, *111*, A07S07, doi:10.1029/2005JA011436.

Dessler, A., and R. Karplus (1961), Some effects of diamagnetic ring currents on Van Allen radiation, *J. Geophys. Res.*, *66*(8), 2289–2295.

Elkington, S. R., M. K. Hudson, and A. A. Chan (1999), Acceleration of relativistic electrons via drift–resonant interaction with toroidal-mode Pc-5 oscillations, *Geophys. Res. Lett.*, *26*(21), 3273–3276.

Engebretson, M., K. H. Glassmeier, M. Stellmacher, W. J. Hughes, and H. Lühr (1998), The dependence of high-latitude Pc5 wave power on solar wind velocity and on the phase of solar wind streams, *J. Geophys. Res.*, *103*(A11), 26,271–26,283.

Fälthammar, C.-G. (1968), Radial diffusion by violation of the third adiabatic invariant, in *Earth*'s *Particles and Fields*, edited by B. M. McCormac, pp. 157–169, NATO Adv. Stud. Inst., Reinhold, New York.

Fei, Y., A. A. Chan, S. R. Elkington, and M. J. Wiltberger (2006), Radial diffusion and MHD–particle simulations of relativistic electron transport by ULF waves in the September 1998 storm, *J. Geophys. Res.*, *111*, A12209, doi:10.1029/2005JA011211.

Friedel, R. H. W., G. D. Reeves, and T. Obara (2002), Relativistic electron dynamics in the inner magnetosphere—A review, *J. Atmos. Sol. Terr. Phys.*, *64*(2), 265–282, doi:10.1016/S1364-6826(01)00088-8.

Green, J. C., and M. G. Kivelson (2001), A tale of two theories: How the adiabatic response and ULF waves affect relativistic electrons, *J. Geophys. Res.*, *106*(A11), 25,777–25,791.

Greenstadt, E. W., J. V. Olson, P. D. Loewen, H. J. Singer, and C. T. Russell (1979), Correlation of Pc3, 4, and 5 activity with solar wind speed, *J. Geophys. Res.*, *84*(A11), 6694–6696.

Hasegawa, A. (1969), Drift mirror instability in the magnetosphere, *Phys. Fluids*, *12*(12), 2642–2650.

Junginger, H., and W. Baumjohann (1988), Dayside long-period magnetospheric pulsations: Solar wind dependence, *J. Geophys. Res.*, *93*(A2), 877–883.

Kepko, L., H. E. Spence, and H. J. Singer (2002), ULF waves in the solar wind as direct drivers of magnetospheric pulsations, *Geophys. Res. Lett.*, *29*(8), 1197, doi:10.1029/2001GL014405.

Kessel, R. L. (2008), Solar wind excitation of Pc5 fluctuations in the magnetosphere and on the ground, *J. Geophys. Res.*, *113*, A04202, doi:10.1029/2007JA012255.

Kim, H.-J., and A. Chan (1997), Fully adiabatic changes in storm time relativistic electron fluxes, *J. Geophys. Res.*, *102*(A10), 22,107–22,116.

Kozyreva, O., V. Pilipenko, M. J. Engebretson, K. Yumoto, J. Watermann, and N. Romanova (2007), In search of a new ULF wave index: Comparison of Pc5 power with dynamics of geostationary relativistic electrons, *Planet. Space Sci.*, *55*(6), 755–769.

Lee, D. H., and R. L. Lysak (1989), Magnetospheric ULF wave coupling in the dipole model: The impulsive excitation, *J. Geophys. Res.*, *94*(A12), 17,097–17,103.

Li, X., D. N. Baker, M. Temerin, T. E. Cayton, E. G. D. Reeves, R. A. Christensen, J. B. Blake, M. D. Looper, R. Nakamura, and S. G. Kanekal (1997), Multisatellite observations of the outer zone electron variation during the November 3–4, 1993, magnetic storm, *J. Geophys. Res.*, *102*(A7), 14,123–14,140.

Mann, I. R., A. N. Wright, K. J. Mills, and V. M. Nakariakov (1999), Excitation of magnetospheric waveguide modes by magnetosheath flows, *J. Geophys. Res.*, *104*(A1), 333–353.

Mann, I., T. P. O'Brien, and D. K. Milling (2004), Correlations between ULF wave power, solar wind speed, and relativistic electron flux in the magnetosphere: solar cycle dependence, *J. Atmos. Sol. Terr. Phys.*, *66*, 187–198, doi:10.1016/j.jastp.2003.10.002.

Mathie, R. A., and I. R. Mann (2000a), A correlation between extended intervals of ULF wave power and storm-time geosynchronous relativistic electron flux measurements, *Geophys. Res. Lett.*, *27*(20), 3261–3264.

Mathie, R. A., and I. R. Mann (2000b), Observations of Pc5 field line resonance azimuthal phase speeds: A diagnostic of their excitation mechanism, *J. Geophys. Res.*, *105*(A5), 10,713–10,728.

Matsuoka, H., K. Takahashi, K. Yumoto, B. J. Anderson, and D. G. Sibeck (1995), Observation and modeling of compressional Pi3 magnetic pulsations, *J. Geophys. Res.*, *100*(A7), 12,103–12,115.

McComas, D. J., S. J. Bame, P. Barker, W. C. Feldman, J. L. Phillips, P. Riley, and J. W. Griffee (1998), Solar Wind Electron Proton Alpha Monitor (SWEPAM) for the advanced composition explorer, *Space Sci. Rev.*, *86*(1–4), 563–612, doi:10.1023/A:1005040232597.

Mills, K., and A. Wright (1999), Azimuthal phase speeds of field line resonances driven by Kelvin–Helmholtz unstable waveguide modes, *J. Geophys. Res.*, *104*(A10), 22,667–22,677.

Mills, K. J., A. N. Wright, and I. R. Mann (1999), Kelvin–Helmholtz driven modes of the magnetosphere, *Phys. Plasmas*, *6*(10), 4070–4087.

Mills, K. J., A. W. Longbottom, A. N. Wright, and M. S. Ruderman (2000), Kelvin–Helmholtz instability on the magnetospheric flanks: An absolute and convective instability approach, *J. Geophys. Res.*, *105*(A12), 27,685–27,699.

Nishimura, Y., A. Shinbori, T. Ono, M. Iizima, and A. Kumamoto (2007), Evolution of ring current and radiation belt particles under the influence of storm-time electric fields, *J. Geophys. Res.*, *112*, A06241, doi:10.1029/2006JA012177.

O'Brien, T. P., R. L. McPherron, D. Sornette, G. D. Reeves, R. Friedel, and H. J. Singer (2001), Which magnetic storms produce relativistic electrons at geosynchronous orbit?, *J. Geophys. Res.*, *106*(A8), 15,533–15,544.

O'Brien, T. P., K. R. Lorentzen, I. R. Mann, N. P. Meredith, J. B. Blake, J. F. Fennell, M. D. Looper, D. K. Milling, and R. R. Anderson (2003), Energization of relativistic electrons in the presence of ULF power and MeV microbursts: Evidence for dual ULF and VLF acceleration, *J. Geophys. Res.*, *108*(A8), 1329, doi:10.1029/2002JA009784.

Ogilvie, K. W., and R. J. Fitzenreiter (1989), The Kelvin–Helmholtz instability at the magnetopause and inner boundary layer surface, *J. Geophys. Res.*, *94*(A11), 15,113–15,123.

Paulikas, G. A., J. B. Blake (1979), Effects of the solar wind on magnetospheric dynamics: Energetic electrons at the synchronous orbit, in *Quantitative Modeling of Magnetospheric Processes, Geophysical Monograph*, vol. 21, edited by W. P. Olson pp. 180–202, AGU, Washington, D. C.

Perry, K. L., M. K. Hudson, and S. R. Elkington (2005), Incorporating spectral characteristics of Pc5 waves into three-dimensional radiation belt modeling and the diffusion of relativistic electrons, *J. Geophys. Res.*, *110*, A03215, doi:10.1029/2004JA010760.

Posch, J. L., M. J. Engebretson, V. A. Pilipenko, W. J. Hughes, C. T. Russell, and L. J. Lanzerotti (2003), Characterizing the long-period ULF response to magnetic storms, *J. Geophys. Res.*, *108*(A1), 1029, doi:10.1029/2002JA009386.

Pu, Z.-Y., and M. G. Kivelson (1983), Kelvin–Helmholtz instability at the magnetopause: Solution for compressible plasmas, *J. Geophys. Res.*, *88*(A2), 841–852.

Reeves, G. D., K. L. McAdams, R. H. W. Friedel, and T. P. O'Brien (2003), Acceleration and loss of relativistic electrons during geomagnetic storms, *Geophys. Res. Lett.*, *30*(10), 1529, doi:10.1029/2002GL016513.

Rostoker, G., S. Skone, and D. N. Baker (1998), On the origin of relativistic electrons in the magnetosphere associated with some geomagnetic storms, *Geophys. Res. Lett.*, *25*(19), 3701–3704.

Samson, J. C., B. G. Harrold, J. M. Ruohoniemi, R. A. Greenwald, and A. D. M. Walker (1992), Field line resonance associated with MHD waveguides in the magnetosphere, *Geophys. Res. Lett.*, *19*(5), 441–444.

Sarafopoulos, D. V. (1995), Long duration Pc5 compressional pulsations inside the Earth's magnetotail lobes, *Ann. Geophys.*, *13*, 926–937.

Shue, J.-H., et al. (1998), Magnetopause location under extreme solar wind conditions, *J. Geophys. Res.*, *103*(A8), 17,691–17,700.

Singer, H. J., L. Matheson, R. Grubb, A. Newman, and S. D. Bouwer (1996), Monitoring space weather with the GOES magnetometers, in *GOES-8 and Beyond, Proc. SPIE Int. Soc. Opt. Eng.*, vol. 2812, edited by E. R. Washwell, pp. 290.

Southwood, D. J. (1968), The hydromagnetic stability of the magnetopause boundary, *Planet. Space Sci.*, *16*, 587–605.

Southwood, D. J. (1974), Some features of field line resonances in the magnetosphere, *Planet. Space Sci.*, *22*, 483–491.

Southwood, D. J. (1976), A general approach to low-frequency instability in the ring current plasma, *J. Geophys. Res.*, *81*(19), 3340–3348.

Southwood, D. J., and M. G. Kivelson (1990), The magnetohydrodynamic response of the magnetospheric cavity to changes in solar wind pressure, *J. Geophys. Res.*, *95*(A3), 2301–2309.

Takahashi, K., and A. Y. Ukhorskiy (2007), Solar wind control of Pc5 pulsation power at geosynchronous orbit, *J. Geophys. Res.*, *112*, A11205, doi:10.1029/2007JA012483.

Takahashi, K., D. G. Sibeck, P. T. Newell, and H. E. Spence (1991), ULF waves in the low-latitude boundary layer and their relationship to magnetospheric pulsations: A multisatellite observation, *J. Geophys. Res.*, *96*(A6), 9503–9519.

Tsyganenko, N. A. (1989), A magnetospheric magnetic field model with a warped tail current sheet, *Planet. Space Sci.*, *37*, 5–20.

Ukhorskiy, A. Y., and M. I. Sitnov (2008), Radial transport in the outer radiation belt due to global magnetospheric compressions, *J. Atmos. Sol. Terr. Phys.*, in press.

Ukhorskiy, A. Y., K. Takahashi, B. J. Anderson, and H. Korth (2005), Impact of toroidal ULF waves on the outer radiation belt electrons, *J. Geophys. Res.*, *110*, A10202, doi:10.1029/2005JA011017.

Ukhorskiy, A. Y., B. J. Anderson, K. Takahashi, and N. A. Tsyganenko (2006a), Impact of ULF oscillations in solar wind dynamic pressure on the outer radiation belt electrons, *Geophys. Res. Lett.*, *33*, L06111, doi:10.1029/2005GL024380.

Ukhorskiy, A. Y., B. J. Anderson, P. C. Brandt, and N. A. Tsyganenko (2006b), Storm time evolution of the outer radiation belt: Transport and losses, *J. Geophys. Res.*, *111*, A11S03, doi:10.1029/2006JA011690.

Vassiliadis, D., I. R. Mann, S. F. Fung, and X. Shao (2007), Ground Pc3–Pc5 wave power distribution and response to solar wind velocity variations, *Planet. Space Sci.*, *55*(6), 743–754, doi:10.1016/j.pss.2006.03.012.

Waters, C. L., K. Takahashi, D. H. Lee, and B. J. Anderson (2002), Detection of ultralow-frequency cavity modes using spacecraft data, *J. Geophys. Res.*, *107*(A10), 1284, doi:10.1029/2001JA000224.

Wolfe, A., and A. Meloni (1981), ULF geomagnetic power near L = 4, 6, relationship to upstream solar wind quantities, *J. Geophys. Res.*, *86*(A9), 7507–7512.

Wright, A. N., and I. Mann (2006), Global MHD eigenmodes of the outer magnetosphere, in *Magnetospheric ULF Waves: Synthesis and New Directions, Geophysical Monograph*, vol. 169, edited by K. Takahashi et al., pp. 51–72, AGU, Washington, D. C.

Wright, A. N., and G. J. Rickard (1995a), A numerical study of resonant absorption in a magnetohydrodynamci cavity driven by a broadband spectrum, *Astrophys. J.*, *444*, 458–470.

Wright, A., and G. Rickard (1995b), ULF pulsations driven by magnetopause motions: Azimuthal phase characteristics, *J. Geophys. Res.*, *100*(A12), 23,703–23,710.

Wright, A., K. Mills, M. Ruderman, and L. Brevdo (2000), The absolute and convective instability of the magnetospheric flanks, *J. Geophys. Res.*, *105*(A1), 385–393.

Wright, A. N., K. J. Mills, A. W. Longbottom, and M. S. Ruderman (2002), The nature of convectively unstable waveguide mode disturbances on the magnetospheric flanks, *J. Geophys. Res.*, *107*(A9), 1242, doi:10.1029/2001JA005091.

K. Takahashi and A. Y. Ukhorskiy, Applied Physics Laboratory, Johns Hopkins University, 11100 Johns Hopkins Road, Laurel, MD 20723-6099, USA. (kazue.takahashi@jhuapl.edu)